Evidence for overdensity around $z_{em} > 4$ quasars from the proximity effect[★]

R. Guimarães,[1,2]† P. Petitjean,[2,3] E. Rollinde,[2] R. R. de Carvalho,[4] S. G. Djorgovski,[5] R. Srianand,[6] A. Aghaee[2,7] and S. Castro[5,8]

[1]*Observatorio Nacional – MCT, R. Gal. José Cristino 77, 20921-400 Rio de Janeiro, RJ, Brazil*
[2]*Institut d'Astrophysique de Paris & Université Pierre et Marie Curie, 98 bis boulevard d'Arago, 75014 Paris, France*
[3]*LERMA, Observatoire de Paris, 61 avenue de l'Observatoire, 75014 Paris, France*
[4]*Instituto Nacional de Pesquisas Espaciais (INPE), Av. dos Astronautas 1758, 12227-010 S. J. dos Campos, SP, Brazil*
[5]*Palomar Observatory, California Institute of Technology, 105-24, Pasadena, CA 91125, USA*
[6]*Inter University Centre for Astronomy and Astrophysics (IUCAA), Post bag 4, Ganeshkhind, Pune 411007, India*
[7]*Department of Physics, University of Sistan and Baluchestan, 98135 Zahedan, Iran*
[8]*European Southern Observatory, Karl–Schwarzschild Strasse 2, Garching, Germany*

ABSTRACT

We study the density field around $z_{em} > 4$ quasars using high-quality medium spectral resolution Echelle Spectrograph and Imager–Keck spectra ($R \sim 4300$, signal-to-noise ratio (S/N) > 25) of 45 high-redshift quasars selected from a total of 95 spectra. This large sample considerably increases the statistics compared to previous studies. The redshift evolution of the mean photoionization rate and the median optical depth of the intergalactic medium (IGM) are derived statistically from the observed transmitted flux and the pixel optical depth probability distribution function, respectively. This is used to study the so-called proximity effect, that is, the observed decrease of the median optical depth of the IGM in the vicinity of the quasar caused by enhanced photoionization rate due to photons emitted by the quasar. We show that the proximity effect is correlated with the luminosity of the quasars, as expected. By comparing the observed decrease of the median optical depth with the theoretical expectation, we find that the optical depth does not decrease as rapidly as expected when approaching the quasar if the gas in its vicinity is part of the standard IGM. We interpret this effect as revealing gaseous overdensities on scales as large as $\sim 15 \, h^{-1}$ Mpc. The mean overdensity is of the order of 2 and 5 within, respectively, 10 and 3 h^{-1} Mpc. If true, this would indicate that high-redshift quasars are located in the centre of overdense regions that could evolve with time into massive clusters of galaxies. The overdensity is correlated with luminosity: brighter quasars show higher overdensities.

Key words: methods: data analysis – methods: statistical – galaxies: clusters: general – intergalactic medium – quasars: absorption lines – dark matter.

1 INTRODUCTION

The intergalactic medium (IGM) has been intensively studied using the absorption seen in the spectra of quasi-stellar objects (QSOs) over a large redshift range ($0.16 \leqslant z_{em} \leqslant 6.3$). This absorption, first identified by Lynds (1971), breaks up at high spectral resolution in hundreds of discrete absorption lines from, predominantly, H I Lyman ultraviolet (UV) resonance lines redshifted in a expanding universe (the so-called Lyα forest; see Rauch 1998 for a review).

The Lyα forest was interpreted by Sargent et al. (1980) as the signature of intervening H I clouds of cosmological nature embedded in a diffuse hot medium. The clouds were further described by Rees (1986) as gravitationally confined by dark matter mini haloes. The advent of numerical simulations has introduced a new and more general scheme in which the IGM is a crucial element of large-scale structures and galaxy formation. It is now believed that the space distribution of the gas traces the potential wells of the dark matter. In addition, most of the baryons are in the IGM at high redshift, making the IGM the reservoir of gas for galaxy formation. The numerical N-body simulations have been successful at reproducing the observed characteristics of the Lyα forest (e.g. Cen et al. 1994; Petitjean, Mücket & Kate 1995; Hernquist, Katz & Weinberg 1996;

Theuns et al. 1998). The IGM is therefore seen as a smooth pervasive medium which can be used to study the spatial distribution of the mass on scales larger than the Jeans' length. This idea is reinforced by observations of multiple lines of sight (e.g. Coppolani et al. 2006).

It is well known that the characteristics of the Lyα forest change in the vicinity of the quasar due to the additional ionizing flux produced by the quasar. The mean neutral hydrogen fraction decreases when approaching the quasar. Because the amount of absorption in the IGM is, in general, increasing with redshift, this reversal in the cosmological trend for redshifts close to the emission redshift of the quasar is called the 'inverse' or 'proximity' effect (Carswell et al. 1982; Murdoch et al. 1986). It is possible to use this effect, together with a knowledge of the quasar luminosity and its position, to derive the mean flux of the UV background if one assumes that the redshift evolution of the density field can be extrapolated from far away to close to the quasar. Indeed, the strength of the effect depends on the ratio of the ionization rates from the quasar and the UV background, and because the quasar's ionization rate can be determined directly through the knowledge of its luminosity and distance, the ionization rate in the IGM can be inferred. This method was pioneered by Bajtlik, Duncan & Ostriker (1988) but more recent data have yielded a wide variety of estimates (Lu, Wolfe & Turnshek 1991; Kulkarni & Fall 1993; Bechtold 1994; Cristiani et al. 1995; Fernandez-Soto et al. 1995; Giallongo et al. 1996; Srianand & Khare 1996; Cooke, Espey & Carswell 1997; Scott et al. 2000, 2002; Liske & Williger 2001). Scott et al. (2000) collected estimates from the literature which vary over almost an order of magnitude at $z = 3$. The large scatter in the results can be explained by errors in the continuum placement, cosmic variance, redshift determination, etc.

In the standard analysis of the proximity effect it is assumed that the underlying matter distribution is not altered by the presence of the quasar. The only difference between the gas close to the quasar or far away from it is the increased photoionization rate in the vicinity of the QSO. If true, the strength of the proximity effect should correlate with the quasar luminosity but such a correlation has not been convincingly established (see Lu et al. 1991; Bechtold 1994; Srianand & Khare 1996; see, however, Liske & Williger 2001). It is in fact likely that the quasars are located inside overdense regions. Indeed, the presence of Lyα absorption lines with $z_{abs} > z_{em}$ suggests an excess of material around QSOs (Loeb & Eisenstein 1995; Srianand & Khare 1996). Furthermore, in hierarchical models of galaxy formation, the supermassive black holes that are thought to power quasars are located in massive haloes (Magorrian et al. 1998; Ferrarese 2002), that are strongly biased to high-density regions. Possible evidence for overdensities around quasars comes also from studies of the transverse proximity effect by Croft (2004), Schirber, Miralda-Escudé & McDonald (2004) and Worseck & Wisotzki (2006) who suggest that the observed absorption is larger than that predicted by models assuming standard proximity effect and isotropic quasar emission. However, in the case of transverse observations, it could be that the quasar light is strongly beamed in our direction or, alternatively, that the quasar is highly variable. Interestingly, neither of these affects the longitudinal proximity effect discussed in the present paper.

Observations of the IGM transmission close to Lyman break galaxies (LBGs) seem to show that, close to the galaxy, the IGM contains more neutral hydrogen than on average (Adelberger et al. 2003). As the UV photons from the LBGs cannot alter the ionization state of the gas at large distances, it is most likely that the excess absorption is caused by the enhanced IGM density around LBGs. It is worth noting, however, that various hydrodynamical simulations have trouble reproducing this so-called galaxy proximity effect (e.g. Bruscoli et al. 2003; Kollmeier et al. 2003; Maselli et al. 2004; Desjacques et al. 2004).

In a recent paper, Rollinde et al. (2005) presented a new analysis to infer the density structure around quasars. The method is based on the determination of the cumulative probability distribution function (CPDF) of pixel optical depth, and so avoids the Voigt profile fitting and line counting which is traditionally used (e.g. Cowie & Songaila 1998; Ellison et al. 2000; Aguirre, Schaye & Theuns 2002; Schaye et al. 2003; Aracil et al. 2004; Pieri, Schaye & Aguirre 2006). The evolution in redshift of the optical depth CPDF far away from the quasar is directly derived from the data. This redshift-dependent CPDF is then compared to the CPDF observed close to the quasar to derive the mean density profile around quasars. The method was applied to 20 lines of sight towards quasars at $z_{em} \sim 2$ observed with UV–Visual Echelle Spectrograph/Very Large Telescope (UVES/VLT), and it was found that overdensities of the order of a few are needed for the observations to be consistent with the value of the UV background flux derived from the mean Lyα opacity. In the present paper, we apply the same method to a large sample of 95 quasars at $z_{em} > 4$ observed with the Echelle Spectrograph and Imager (ESI) mounted on the Keck II telescope.

In Section 2, we describe the data and the selection of the sample used in the present work. We derive the redshift evolution of the ionizing UV background and of the median IGM optical depth in Sections 3 and 4, respectively. We discuss the proximity effect in Section 5 and conclude in Section 6. We assume throughout this paper a flat Universe with $\Omega_m = 0.3$, $\Omega_\Lambda = 0.7$, $\Omega_b = 0.04$ and $H_0 = 70 \text{ km s}^{-1}$.

2 DATA AND SAMPLE SELECTION

Medium resolution ($R \sim 4300$) spectra of all $z > 3$ quasars discovered in the course of the DPOSS (Digital Palomar Observatory Sky Survey; see e.g. Kennefick, Djorgovski & de Carvalho 1995; Djorgovski et al. 1999a and the complete listing of QSOs available at http://www.astro.caltech.edu/~george/z4.qsos) have been obtained with the ESI (Sheinis et al. 2002) mounted on the Keck II 10-m telescope. Signal-to-noise ratio (S/N) is usually larger than 15 per 10 km s^{-1} pixel. These data have already been used to construct a sample of damped Lyα (DLA) systems at high redshift (Prochaska et al. 2003a; Prochaska, Castro & Djorgovski 2003b). In total, 95 quasars have been observed.

The Keck/ESI spectra were reduced (bias subtraction, flat-fielding, spectrum extraction) using standard procedures of the IRAF package. The different orders of the spectra were combined using the scombine task. In the Echellette-mode spectra are divided in 10 orders covering the wavelength range: $4000 \leqslant \lambda_{obs} \leqslant 10\,000$ Å. In this work, we use only orders from 3 (centre 4650 Å) to 7 (centre 6750 Å). The spectral resolution is $R \sim 4300$ or ~ 70 km s^{-1}. During the process of combining the orders, we controlled carefully the S/N obtained in each order. Wavelengths and redshifts were computed in the heliocentric rest frame and the spectra were flux calibrated and then normalized.

The S/N per pixel was obtained in the regions of the Lyα forest that are free of absorption and the mean S/N value, averaged between the Lyα and Lyβ emission lines, was computed. We used only spectra with mean S/N $\geqslant 25$. We rejected the broad absorption line (BAL) QSOs and QSOs with more than one DLA system redshifted between the Lyα and the Lyβ emission lines because their presence may overpollute the Lyα forest. Metal absorptions are not subtracted from the spectra. We can estimate that the number of

Table 1. Quasar sample.

| QSO	$z_{em}{}^a$	$z_{em}{}^b$	V_{mag}	S/N	$L_{912}{}^c$ $(h^{-2}\ \mathrm{erg\ s^{-1}\ Hz^{-1}})$
PSS0117+1552	4.241	4.244	18.6	45	4.53×10^{31}
PSS0118+0320	4.235	4.232	18.50	30	4.38×10^{31}
PSS0121+0347	4.130	4.127	17.86	72	6.76×10^{31}
SDSS0127-0045	4.067	4.084	18.37	25	4.04×10^{31}
PSS0131+0633	4.432	4.430	18.24	25	6.88×10^{31}
PSS0134+3307	4.534	4.536	18.82	30	4.73×10^{31}
PSS0209+0517	4.206	4.194	17.36	40	8.16×10^{31}
PSS0211+1107	3.975	3.975	18.12	66	6.14×10^{31}
PSS0248+1802	4.427	4.430	18.4	60	8.32×10^{31}
PSS0452+0355	4.397	4.395	18.80	30	4.77×10^{31}
PSS0747+4434	4.434	4.435	18.06	54	7.98×10^{31}
PSS0808+5215	4.476	4.510	18.82	37	4.29×10^{31}
SDSS0810+4603	4.078	4.074	18.67	43	3.22×10^{31}
PSS0852+5045	4.213	4.216	19	54	2.60×10^{31}
PSS0926+3055	4.188	4.198	17.31	77	1.22×10^{32}
PSS0950+5801	3.969	3.973	17.38	85	9.31×10^{31}
PSS0957+3308	4.283	4.274	17.59	40	9.80×10^{31}
PSS1057+4555	4.127	4.126	17.7	76	7.67×10^{31}
PSS1058+1245	4.332	4.330	18	46	7.45×10^{31}
PSS1140+6205	4.507	4.509	18.73	61	4.77×10^{31}
PSS1159+1337	4.089	4.081	18.50	45	3.65×10^{31}
PSS1248+3110	4.358	4.346	18.9	25	3.19×10^{31}
SDSS1310-0055	4.152	4.151	18.85	38	2.82×10^{31}
PSS1317+3531	4.370	4.369	19.10	28	2.75×10^{31}
J1325+1123	4.408	4.400	18.77	25	4.20×10^{31}
PSS1326+0743	4.121	4.123	17.3	66	1.01×10^{32}
PSS1347+4956	4.597	4.560	17.9	40	1.02×10^{32}
PSS1401+4111	4.008	4.026	18.62	30	2.90×10^{31}
PSS1403+4126	3.862	3.862	18.92	25	1.85×10^{31}
PSS1430+2828	4.309	4.306	19.30	40	2.18×10^{31}
PSS1432+3940	4.291	4.292	18.6	36	4.04×10^{31}
PSS1443+2724	4.419	4.406	19.3	30	2.57×10^{31}
PSS1458+6813	4.295	4.291	18.67	60	5.04×10^{31}
PSS1500+5829	4.229	4.224	18.6	40	3.74×10^{31}
GB1508+5714	4.306	4.304	18.9	32	3.12×10^{31}
PSS1535+2943	3.979	3.972	18.9	29	2.26×10^{31}
PSS1555+2003	4.226	4.228	18.9	31	3.15×10^{31}
PSS1633+1411	4.360	4.349	19.0	43	3.36×10^{31}
PSS1646+5514	4.110	4.084	18.11	37	4.81×10^{31}
PSS1721+3256	4.031	4.040	19.23	43	1.85×10^{31}
PSS1723+2243	4.515	4.514	18.17	42	8.77×10^{31}
PSS2154+0335	4.349	4.359	18.41	26	6.20×10^{31}
PSS2203+1824	4.372	4.375	18.74	34	4.50×10^{31}
PSS2238+2603	4.023	4.031	18.85	24	2.74×10^{31}
PSS2344+0342	4.341	4.340	17.87	30	4.38×10^{31}

[a]Mean of estimates from a Gaussian fit to the C IV emission line and from the peak of the Lyα emission.
[b]Estimate using the IRAF RVIDLINES task.
[c]Continuum luminosity at 912 Å.

intervening C IV and Mg II systems with $W_{obs} > 0.25$ Å is of the order of 5 along each of the lines of sight (see e.g. Boksenberg, Sargent & Rauch 2003; Aracil et al. 2004; Tytler et al. 2004; Scannapieco et al. 2006). This means we expect an error on the determination of the mean absorption of the order of 1 per cent. This is at least five times smaller than the error expected from the placement of the continuum.

In Table 1, we give the characteristics of the forty-five QSO spectra satisfying the above criteria that are used in the present work. Column 1: the QSO's name; Column 2: the emission redshift esti-
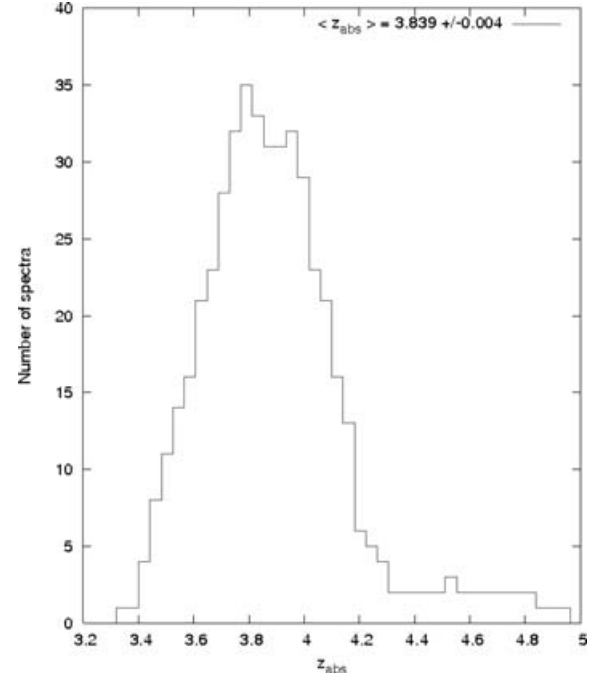
Figure 1. Number of spectra in our sample contributing to the study of the Lyα forest at a given redshift as a function of redshift.

mated as the average of the determinations of the peak of the Lyα emission and the peak of a Gaussian fitted to the C IV emission line; Column 3: the emission redshift obtained using the IRAF task RVIDLINES (see Section 5.1); Column 4: the apparent V magnitude; Column 5: the mean S/N in the Lyα forest; and Column 6: the intrinsic luminosity at the Lyman limit estimated from the V-magnitude assuming that the QSO continuum spectrum is a power law of index -0.6 (see Section 5). In Fig. 1, we show the histogram of the number of spectra in our sample contributing to the study of the Lyα forest at a given redshift as a function of redshift. Normalization of the spectra is known to be a crucial step in these studies. An automatic procedure (Aracil et al. 2004) estimates iteratively the continuum by minimizing the sum of a regularization term (the effect of which is to smooth the continuum) and a χ^2 term, which is computed from the difference between the quasar spectrum and the continuum estimated during the previous iteration. Absorption lines are avoided when computing the continuum. A few obvious defects are then corrected by hand adjusting the reference points of the fit. This happens to be important near the peak of strong emission lines and overdamped absorption lines. The automatic method works very well, and a minimal manual intervention is necessary. The procedure was calibrated by Aracil et al. (2004) using simulated quasar spectra (with emission and absorption lines) adding continuum modulations to mimic an imperfect correction of the blaze along the orders and noise to obtain a S/N similar to that in the data. We noted that the procedure underestimates the true continuum in the Lyα forest by a quantity depending smoothly on the wavelength and the emission redshift by an amount of about 3–5 per cent at $z \sim$ 3.5–4. (see fig. 1 of Aracil et al. 2004). This is less than our typical errors and therefore we did not correct the normalized spectra for this. Note that, due to strong blending, errors can be as high as 10 per cent in places (see also Croft et al. 2002; Becker, Rauch & Sargent 2006; McDonald et al. 2006; Desjacques, Nusser & Sheth 2007). In that case, however, the optical depth will be usually larger
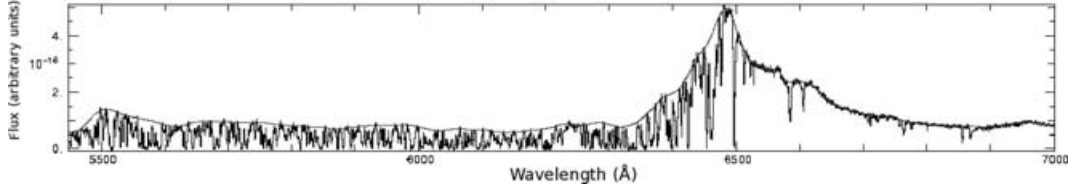
Figure 2. Flux-calibrated spectrum of PSS 1058+1245. The continuum derived automatically is overplotted.

than the limit we will used to reject pixels badly affected by saturation. It must be noted also that, because of the reduced absorption in the vicinity of the quasar, the continuum determination is more reliable in the wing of the Lyα emission line. The normalization procedure we have used is preferred to other methods that are more arbitrary. It is completely reproducible and introduces only a small systematic error that we can control. A final sample reduced spectrum with the continuum fitting is shown in Fig. 2.

3 THE IONIZING BACKGROUND RADIATION FIELD

The standard treatment of the proximity effect consists in studying the evolution of the mean absorption in the Lyα forest when approaching the quasar. Far away from the quasar the only source of ionizing photons is the UV background whereas in the vicinity of the quasar, the gas is ionized by both the UV background and the QSO. Assuming (i) that the luminosity of the quasar is known, (ii) that the distance from the gas to the quasar is cosmological (and therefore given by the difference in redshift) and (iii) that the density field in the IGM is not modified by the presence of the quasar, it is possible to derive observationally the distance to the quasar where the ionizing flux from the quasar equals the flux from the UV background. This, in turn, gives an estimate of the UV background flux. The last assumption neglects the fact that quasars can be surrounded by significant overdensities (e.g. Pascarelle et al. 2001; Adelberger et al. 2003; Rollinde et al. 2005; Kim & Croft 2006; Faucher-Giguere et al. 2007).

However, the above approach can be reversed to derive the density distribution around the quasar if the UV background can be estimated from elsewhere. Actually, it is possible to estimate this flux by modelling the redshift evolution of the mean absorption in the IGM. For $z > 4$ we can follow Songaila & Cowie (2002) and use the mean normalized transmitted flux, $F(z)$, to derive the normalized ionization rate, g, in units of 10^{-12} s^{-1}, by inverting the following equation (see also McDonald & Miralda-Escudé 2001; Cen & Mc Donald 2002):

$$F(z) = 4.5g^{-0.28}\left[\frac{(1+z)}{7}\right]^{2.2} e^{\left\{-4.4g^{-0.4}\left[\frac{(1+z)}{7}\right]^3\right\}} \tag{1}$$

with

$$g \equiv \Gamma_{-12} T_4^{0.75} h \left(\frac{\Omega_m}{0.35}\right)^{0.5} \left(\frac{\Omega_b h^2}{0.0325}\right)^{-2}. \tag{2}$$

Applying the above equations, we can derive the redshift dependence of Γ_{-12} from the observed transmitted flux (for $z > 4$). For this, we have used the Lyα forest over the rest-wavelength range 1070–1170 Å to avoid contamination by the proximity effect close to the Lyα emission line and by possible O VI associated absorbers. We also carefully avoided regions flagged because of data reduction problems or DLA absorption lines. We divided each spectrum in
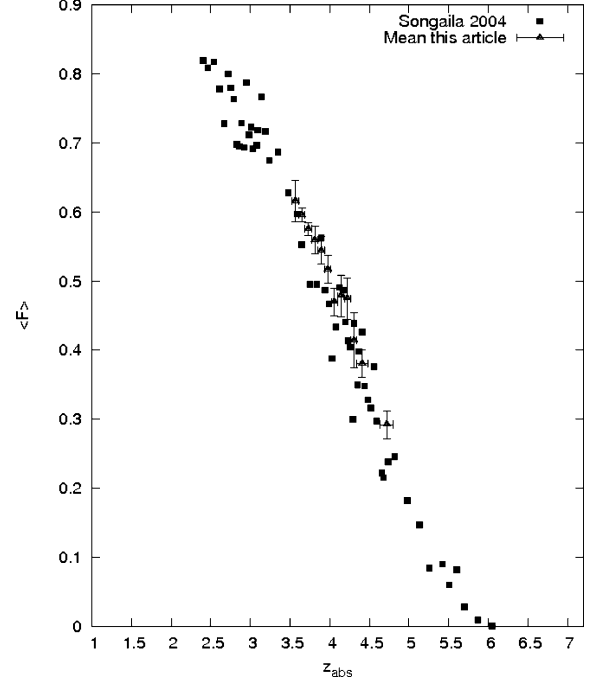

Figure 3. The observed normalized transmitted flux $\langle F \rangle$ as a function of redshift.

bins of length 50 Å in the observed frame, corresponding to about $\triangle z = 0.04$. The mean transmitted flux was calculated as the mean flux over all pixels in a bin. At each redshift, we then averaged the transmitted fluxes over all spectra covering this redshift. Errors were estimated as the standard deviation of the mean values divided by the square root of the number of spectra. The corresponding scatter in the transmitted flux cannot be explained by photon noise or by uncertainties in the continuum, suggesting that errors are dominated by cosmic variance. The mean transmitted flux that we have obtained is plotted in Fig. 3 together with results by Songaila (2004).

The normalized ionization rate defined in equation (2) is derived from the mean normalized transmitted flux by inverting equation (1). Results are plotted in Fig. 4. To decrease the errors, we have used only three bins at $z > 4$. It can be seen that our measurements are consistent with those by McDonald et al. (2000) at lower redshift. Fitting both McDonald's and our results together, we find that the redshift evolution of g is described as $g = 1.11[(1 + z)/6]^{-1.63}$. Note that our fit is not consistent with the results by Songaila (2004) who find $g = 0.74[(1 + z)/6]^{-4.1}$ for $z > 4$. The corresponding photoionization rate, Γ_{-12}, in units of 10^{-12} s^{-1}, is given in Fig. 5, assuming $\Omega_b h^2 = 0.019$, $\Omega_m = 0.3$ and three different values of gas temperature $T_4 = 1, 1.5$ and 2, in units of 10^4 K. These results are consistent with the measurements by McDonald & Miralda-Escudé (2001) for a mean temperature of $T_4 \sim 1.5$–2 which is the
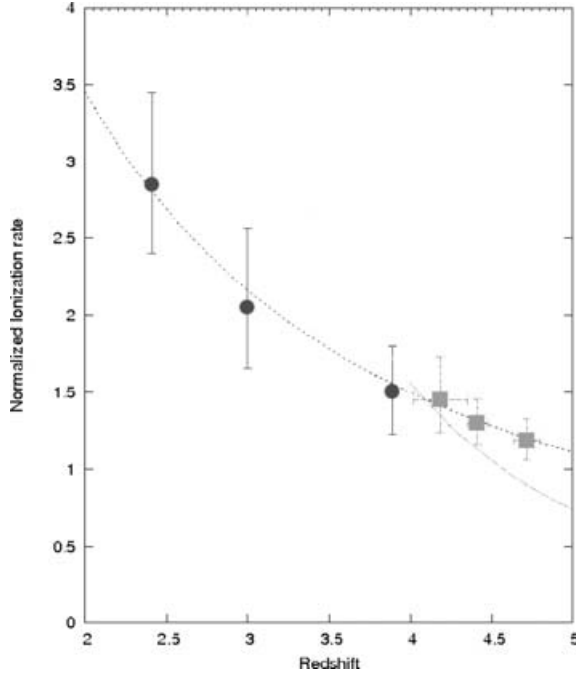
mean temperature expected in the IGM at these redshifts. However, recent determination of this quantity (Becker et al. 2006) using a lognormal distribution for the optical depth distribution indicate that Γ_{-12} could be higher by about a factor of 2–3 at these redshifts. We therefore have used in the following a mean temperature of $T_4 = 1$.

4 THE LYα OPTICAL DEPTH STATISTICS IN THE IGM

To study the influence of the additional ionizing flux from the quasar on the Lyα optical depth, we have first to derive the evolution of the optical depth with redshift in the IGM at large distances from the quasar. The observed H I opacity is simply

$$\tau_{\rm H I}(\lambda) = -\ln\left(\frac{F_{\lambda_{\rm obs}}}{F_{\lambda_{\rm cont}}}\right), \qquad (3)$$

where $F_{\lambda_{\rm obs}}$ is the observed flux and $F_{\lambda_{\rm cont}}$ is the flux in the continuum. Its evolution with redshift is described as

$$\tau \propto (1+z)^{\alpha}. \qquad (4)$$

For each spectrum of the sample we estimate the optical depth, τ, in each pixel between $\tau_{\rm min} = -\ln(1-3\sigma)$ and $\tau_{\rm max} = -\ln(3\sigma)$, where $\sigma(\lambda)$ is the rms of the noise measured in the spectrum (see Column 5 of Table 1). We then construct the cumulative probability distribution of τ (CPDF) in redshift windows of approximately $\triangle z = 0.04$ corresponding to 50 Å in the observed frame and estimate the associated percentiles. Because low and high values of the optical depth are lost either in the noise or because of saturation, we can use only the intermediate values of the percentiles. The evolutions with redshift of the 40, 50, 60 and 70 per cent percentiles are given in Fig. 6.

The redshift evolution index in equation (4) can be derived from the redshift evolution of the percentiles of the pixel optical depth CPDF (see Rollinde et al. 2005). The values obtained for α are
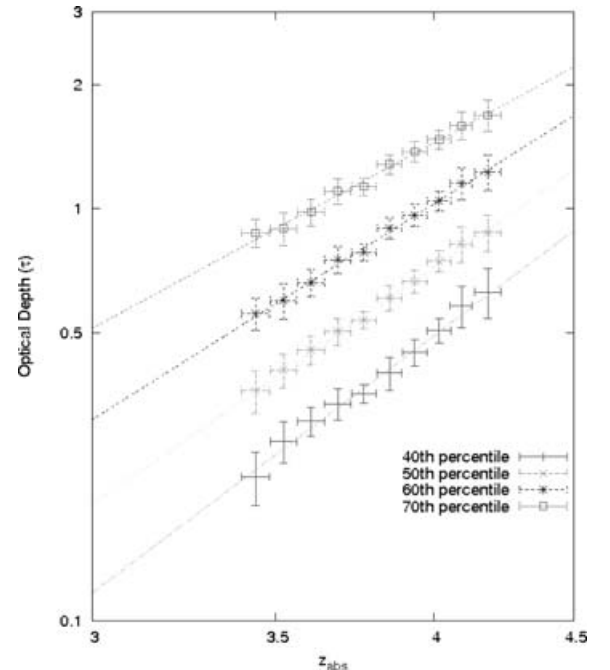

Figure 4. The normalized ionization rate obtained from the transmitted flux observed in our data by inverting equation (1) in three redshift bins (filled squares) at $z > 4$. Filled circles are the measurements of McDonald et al. (2000) for lower redshift. The dotted line is a power law of the form $1.11[(1+z)/6]^{-1.63}$ fitted to the data of McDonald et al. (2000) and this paper. The dashed line is a power law of the form $0.74[(1+z)/6]^{-4.1}$ obtained, for $z > 4$, by Songaila (2004).
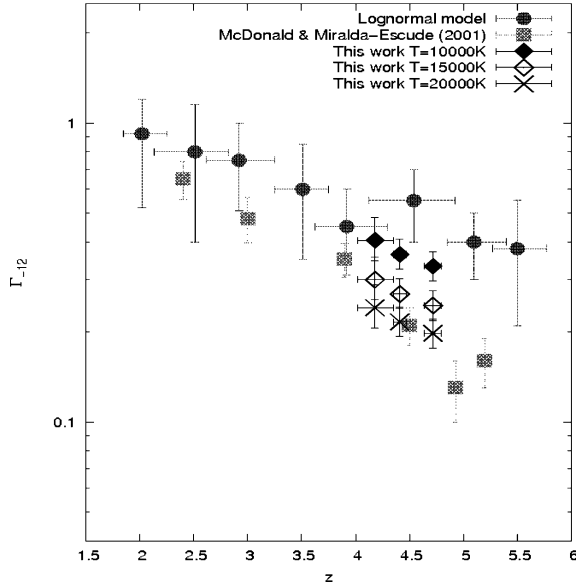
Figure 5. Redshift evolution of the photoionization rate, Γ_{-12}, derived from our data and using three different temperatures for the IGM, $T_4 = 1.0$, 1.5 and 2, in units of 10^4 K (filled diamond, open diamond and crosses, respectively). Filled squares show the results by McDonald & Miralda-Escudé (2001), and filled circles show the results from Becker et al. (2006). $\Omega_b\, h^2 = 0.019$, $\Omega_m = 0.3$ are assumed here.

Figure 6. Redshift evolution of different percentiles derived from the CPDF of the pixel optical depth.
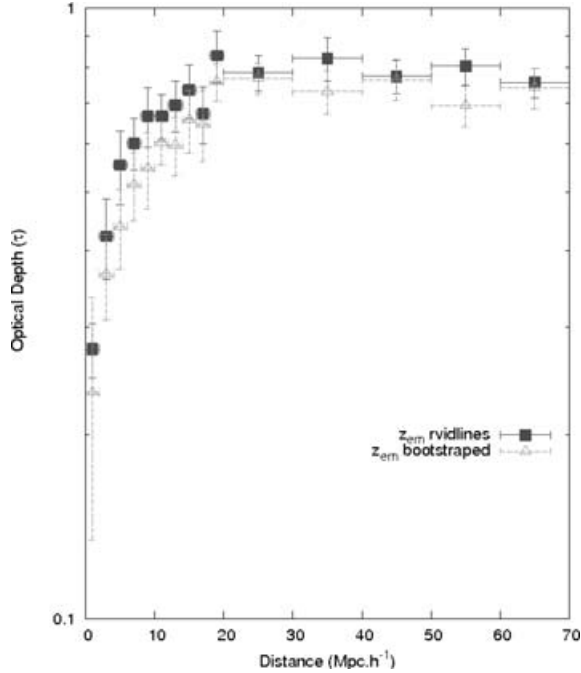
Figure 7. The median optical depth corrected for redshift evolution [$\tau \propto (1 + z)^\alpha$ with $\alpha = 4.8$] is given versus the distance to the quasar, derived using QSO emission redshifts from Column 3 of Table 1 (filled squares). Open triangles correspond to the case where these redshifts are increased by an amount taken randomly between 0 and 1500 km s^{-1}.

(5.8 ± 0.5) for the 40 per cent percentile, (5.1 ± 0.2) for the 50 per cent percentile, (4.3 ± 0.2) for the 60 per cent percentile and (3.8 ± 0.4) for the 70 per cent percentile. We use throughout the rest of the paper $\alpha = 4.8$.

5 THE PROXIMITY EFFECT FROM OPTICAL DEPTH STATISTICS

The evolution with redshift of the optical depth in the IGM is inverted in the vicinity of the quasar due to the additional ionizing flux from the quasar. To disentangle the two effects we can correct the observed optical depth for the redshift evolution in the absence of the quasar by replacing τ_i at redshift z_i by $\tau_i[(1 + z_{ref})/(1 + z_i)]^\alpha$, where z_{ref} is a fixed redshift taken as reference. We have corrected the observed optical depth for each pixel using the factor above with $z_{ref} = 4.5$ and the value of α obtained from the redshift evolution of the IGM CPDF, $\alpha = 4.8$. The results are shown in Fig. 7 (filled squares). The observed corrected median optical depth is given versus the distance to the quasar computed using the cosmological parameters given in Section 2 and assuming emission redshifts from Column 3 of Table 1. The proximity effect is apparent as a decrease of the optical depth within a distance to the quasar smaller than ∼15–20 h^{-1} Mpc.

5.1 QSO systemic redshifts

The above effect depends on the accurate determination of the QSO systemic redshift. Gaskell (1982) has shown that the redshifts derived from different quasar emission lines often do not agree with each other within typical measurement errors. The high-ionization broad emission lines (HILs; e.g. Lyα λ1215.67, C IV λ1549, C III λ1909 and N V λ1240) are found systematically

blueshifted with respect to the low-ionization broad emission lines (LILs; e.g. O I λ1305, Mg II λ2798 and the permitted Balmer series) and principally from the forbidden narrow emission lines (e.g. Ne V λ3426, O II λ3727, Ne III λ3870, O III λ5007). The narrow emission lines arise from gas located in the galaxy host and their redshift should be more representative of the centre-of-mass redshift (see e.g. Tytler & Fan 1992; Baker et al. 1994).

Unfortunately, for our sample of quasars with emission redshifts in the range $4 \leqslant z_{em} \leqslant 4.5$, the forbidden narrow emission lines cannot be detected from the ground because they are redshifted in near-infrared spectral windows that are absorbed by the terrestrial atmosphere. We have derived the emission redshifts using two approaches. In the first approach, the final redshift (see Column 2 of Table 1) is the mean of two estimates: one obtained by fitting a Gaussian to the C IV emission line and the other by measuring the peak of the Lyα emission line to avoid the various absorption features shortwards of the line. In the second approach, the emission redshift (see Column 3 of Table 1) was obtained using the IRAF task RVIDLINES. Initially, we identify a prominent spectral feature (usually the Lyα emission line) to which a Gaussian function is fitted. Based on the central wavelength of this line and an input list of known spectral features, other features at a consistent redshift are identified and fitted. The final emission redshift is a weighted average value based on the Gaussian fits. The median optical depth of the IGM versus the distance to the quasar computed using emission redshifts obtained by this second approach is shown as squares in Fig. 7.

As we know that HILs are systematically blueshifted, with respect to LILs and narrow emission lines, from 500 to 1500 km s^{-1} (Tytler & Fan 1992), we have increased the emission redshift (obtained by fitting the emission lines) by a random amount and calculated the optical depth versus the distance to the quasar as follows. For each realization, we increase the redshift of each of the 45 quasars by an amount taken randomly between 0 and 1500 km s^{-1}. We calculate the distance of each pixel of the lines of sight to the corresponding quasar and compute the median optical depth for each value of r by averaging over all quasars. We then average the optical depths over a hundred realizations. Errors are taken as the mean rms obtained over the realizations. Results are shown in Fig. 7 (triangles). The proximity effect is more pronounced in that case, as expected. This approach will be used in the next Sections whenever we will use QSO emission redshifts.

5.2 The QSO ionization rate

The strength of the proximity effect depends on the ratio of the ionization rates from the QSO emission and the UV background. The QSO ionization rate can be determined directly from its luminosity. The H I ionization rate due to a source of UV photons is formally given by the equation

$$\Gamma_{QSO} = \int_{\nu_0}^{\infty} \left[4\pi J_{QSO}(\nu) \frac{\sigma_{HI}(\nu)}{h\nu} \right] d\nu (s^{-1}), \qquad (5)$$

where, ν_0 is the frequency of the Lyman limit, $\sigma_{HI}(\nu) = 6.3 \times 10^{-18}(\nu_0/\nu)^3$ cm^2 is the H I photoionization cross-section, $J_{QSO}(\nu) = J_{QSO}(\nu_0) (\nu/\nu_0)^{-\phi}$, if we assume that the ionizing spectrum is a power law of index ϕ and where, $J_{QSO}(\nu_0)$ is defined as

$$4\pi J_{QSO}(\nu_0) = \frac{L_{QSO}}{4\pi r^2}, \qquad (6)$$

with L_{QSO} being the monochromatic luminosity of the quasar at the Lyman limit. These luminosities are computed extrapolating the flux in the continuum at $\lambda_{obs} \sim 6000$ Å using a power law of index $\phi =$
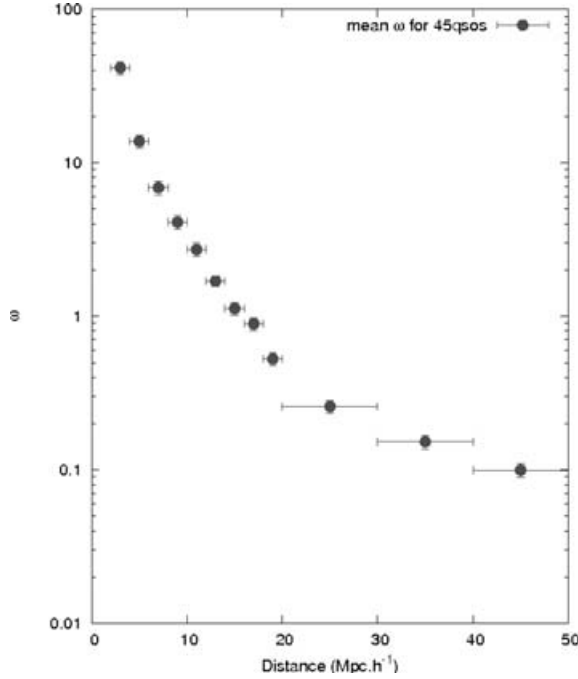
Figure 8. The ratio $\omega = \Gamma_{QSO}/\Gamma_{bck}$ of the ionizing rate from the QSO to that from the UV background versus the cosmological distance between the quasar and the cloud in the IGM. Γ_{bck} is taken from Fig. 5.

−0.6 (Francis, Hooper & Impey 1993). We checked that within a reasonable range of $\phi = -0.5$ to -0.7 (e.g. Cristiani & Vio 1990), our main result (i.e. the density structure around quasars) is not affected by this choice. Therefore,

$$\Gamma_{QSO} = \frac{12.6 \times 10^{-12}}{3 + \phi} J_{QSO}(\nu_0) \, 10^{21} \, (\text{s}^{-1}); \tag{7}$$

thus,

$$\Gamma_{QSO}^{12} = \frac{12.6}{3 + \phi} \frac{L_{QSO}/4\pi}{4\pi r^2} 10^{21} (10^{-12} \, \text{s}^{-1}), \tag{8}$$

where r is the luminosity distance from the quasar of emission redshift z_{em} to the cloud at redshift z and is calculated using equations given by Liske (2003) for a flat cosmological model.

5.3 Ionizing rate ratio

We define ω as the ratio of the ionizing rate due to the quasar emission to that due to the UV background, $\omega = \frac{\Gamma_{QSO}(r,z)}{\Gamma_{bck}(z)}$. The later has been derived in Section 4 (see Fig. 5). The enhanced ionizing flux in the vicinity of the QSO induces a decrease in the optical depth of the IGM observed in the absence of the QSO by a factor $(1 + \omega)$. For each spectrum, we have calculated ω_{QSO} and r for each pixel and then, at a given r, we have derived ω for the whole sample as the median of the individual values $\omega_{QSO}(r)$ found for each of the 45 quasars. The result is shown in Fig. 8.

5.4 Overdensities around the quasar

In the standard analysis of the proximity effect, it is assumed that the matter distribution in the IGM is not altered by the presence of the quasar. The only difference between the gas located either close to the quasar or far away from it is the increased photoionization rate in the vicinity of the quasar. In that case, far away from the quasar,
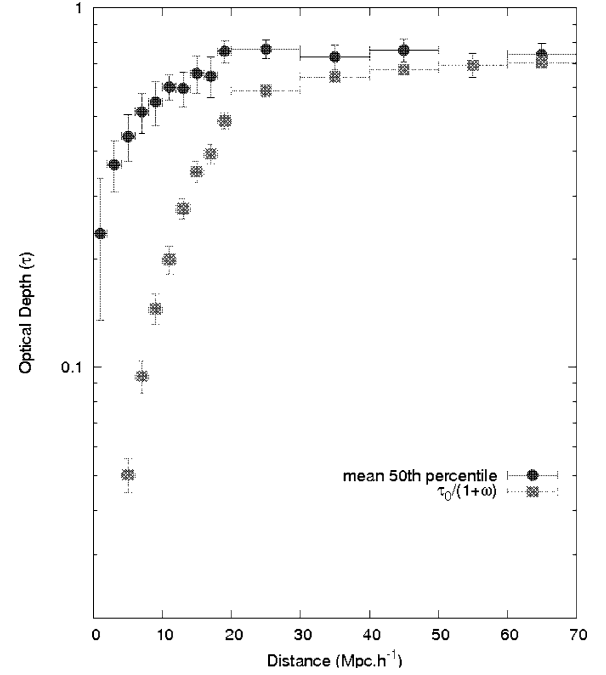

Figure 9. Comparison of median optical depth's evolution observed close to the quasars (filled circles) with that of an evolution due to the ionization field of the quasar only (equation 3; filled squares). The difference between the curves can be interpreted as the presence of an overdensity of gas in the vicinity of the quasar.

the median optical depth corrected for redshift evolution, τ_{median}, should be a constant we can call τ_0. In the vicinity of a QSO, due to the emission of ionizing photons, τ_{median} is no more a constant (see Fig. 7) and decreases when r decreases as

$$\tau_{median} = \tau_0 \frac{1}{(1 + \omega)}, \tag{9}$$

where ω was defined and derived in the previous section (see Fig. 8).

The observed median optical depth τ_{median}^{obs} is compared to $\tau_0/(1 + \omega)$ in Fig. 9. It is apparent that the two curves do not agree and that the observed median optical depth is much larger than what would be expected in the case the density field of the IGM remains unperturbed when approaching the quasar. This means that on an average, there is an overdensity of gas compared to the IGM in the vicinity of the quasar.

If an overdensity, $\frac{\rho(r)}{\rho_0}$, is present around the quasar, then the median optical depth should be

$$\tau_{median} = \tau_0 \frac{(\rho(r)/\rho_0)^{[2-0.7(\gamma-1)]}}{(1 + \omega)}. \tag{10}$$

The γ exponent has been shown by Schaye et al. (2000) to be in the range $\gamma = [1$–$1.5]$, thus it is reasonable to assume $\gamma = 1$ for this work.

Using equation (3), we can derive the actual overdensity. It is given versus the distance to the quasar in Fig. 10 (filled circles). The gas density close to the quasar is significantly higher than the mean density in the IGM at least within the first $10 \, h^{-1}$ Mpc or so.

6 DISCUSSION AND CONCLUSIONS

In this paper, we have used the method presented by Rollinde et al. (2005) to probe the density structure around quasars. In the vicinity
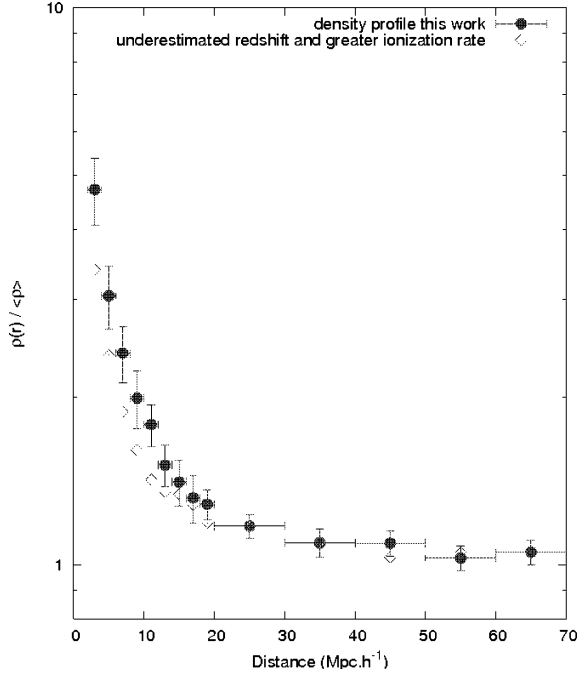
Figure 10. The mean density profile around quasars with emission redshift in the range $4 \leqslant z_{em} \leqslant 4.5$ as derived from this work is shown as filled circles. Open diamonds indicate the lower limit on the density profile derived assuming that the redshift from Column 3 Table 1 is systematically underestimated by 1500 km s^{-1} and that the ionizing rate in the IGM is that measured by Becker et al. (2006).
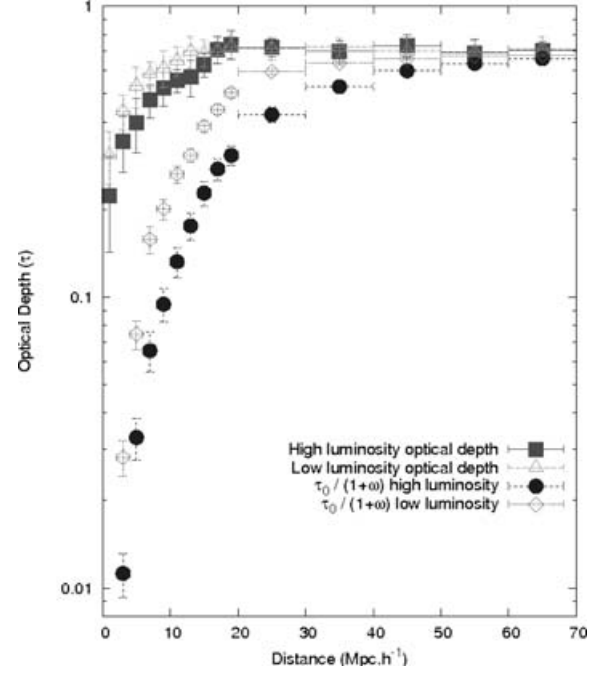

Figure 11. The median optical depth in versus the distance from the cloud to the quasar for two subsets of our QSO sample: one including the 15 QSOs of highest luminosities (filled squares) and the other including the 17 QSOs of lowest luminosities (open triangles). It is apparent that the proximity effect is correlated with luminosity as expected. The curves giving the factor $(1 + \omega)$ are drawn for each subset for illustration (filled circles and open diamonds, respectively.

of the quasar and in comparison with the situation far away from it, the ionization factor of the gas is increased by the emission of ionizing photons by the quasar and is decreased by the presence of an overdensity. If the redshift evolution of the IGM photoionization rate and that of the median optical depth in the IGM are both constrained by the observed evolution of the median optical depth in the Lyα forest far from the quasar, then it is possible to derive the density structure in the vicinity of the quasar. We have followed McDonald & Miralda-Escudé (2001) to derive the mean ionization rate in the IGM at $z > 4$. Our results are lower, by a factor of about 1.5, than the new results by Becker et al. (2006). We then have used the redshift evolution of the pixel optical depth PDF to estimate the redshift evolution of the median optical depth of the IGM. Using these results, we have found that quasars are surrounded by significant overdensities on scales up to about 10 h^{-1} Mpc. The overdensity is of the order of a factor of 2 at 10 h^{-1} Mpc but is larger than five within the first Mpc. If true, we can estimate that the mass surrounding the quasars within 1 Mpc at this redshift is of the order of $10^{14} \, M_{\odot}$ corresponding to the mass of a big cluster of galaxies. An overdensity can be artificially derived from the above analysis if (i) the photoionization rate is underestimated and/or (ii) the redshift of the quasars are systematically underestimated for any reason. To check the robustness of our result, we can try to obtain a lower limit on the overdensity surrounding the quasars. For this we have arbitrarily increased the photoionization rate that we used by a factor of 1.5 so that it is equal to the value obtained by Becker et al. (2006) at the same redshift. In addition, we have increased all quasar emission redshifts by 1500 km s^{-1} to account for a possible systematic underestimate of the emission redshift when using the Lyα emission line (note, however, that in our treatment we already increase the emission redshift from the Lyα emission line by an amount taken

randomly between 0 and 1500 km s^{-1}). The result is shown in Fig. 10 (open diamonds). It can be seen that the overdensity is still present although smaller as expected. If our interpretation of the proximity effect is correct, we should expect a correlation between the strength of the observed proximity effect and the intrinsic luminosity of the QSOs. To test this effect, we have considered two subsets of our quasar sample, one containing the 15 QSOs with highest intrinsic luminosities ($6.14 \times 10^{+31} \leqslant L \leqslant 1.22 \times 10^{+32} \, h^{-2} \, erg \, s^{-1} \, Hz^{-1}$) and the other containing the 17 QSOs with lowest intrinsic luminosities ($1.85 \times 10^{+31} \leqslant L \leqslant 3.74 \times 10^{+31} \, h^{-2} \, erg \, s^{-1} \, Hz^{-1}$). We have avoided quasars with intermediate luminosities because they may dilute the possible result. In Fig. 11, we plot for both subsets the median optical depth versus the distance to the quasar. It is apparent that the proximity effect is less pronounced for the low-luminosity sample compared to the high-luminosity sample as expected. The proximity effect is correlated with QSO luminosities. For illustration, we plot also $\tau_0/(1 + \omega)$ for both subsets on the figure. The corresponding overdensities around the quasars in the two subsets are shown in Fig. 12. The overdensity is correlated with luminosity. Brighter quasars show higher overdensities. Some caution should be applied when interpreting this result, however, as we have used a quite simple model to correct the observed proximity effect.

At redshift $z \sim 2$, Rollinde et al. (2005) claimed tentative detection of overdensities of about a factor of 2 on scales $\sim 5 \, h^{-1}$ Mpc. The result was only marginal because the statistics was small. With a sample of 45 quasars at $z > 4$, we have demonstrated that overdensities exist. This result strongly supports the idea that quasars at high redshift are located in regions of high overdensities probably flagging the places where massive clusters of galaxies will form.
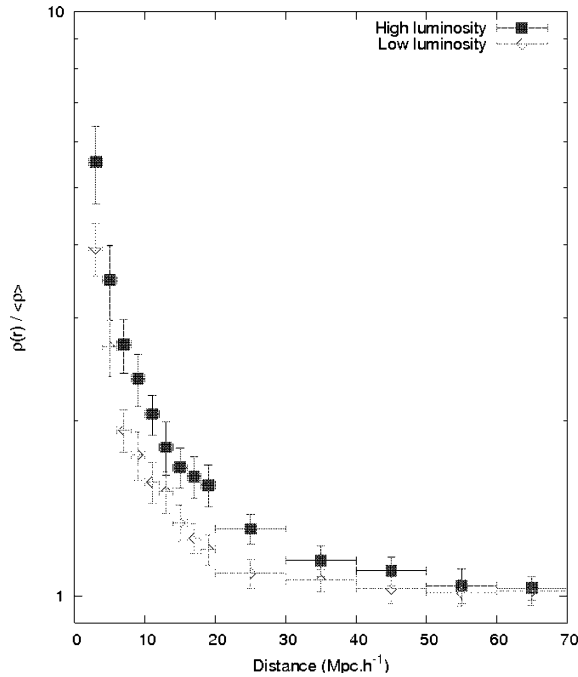
Figure 12. The density profile around quasars versus the distance from the cloud to the quasar for two subsets of our QSO sample: one including the 15 QSOs of highest luminosities (filled squares) and the other including the 17 QSOs of lowest luminosities (open diamonds).

It has been known for a long time that quasars are associated with enhancements in the distribution of galaxies (Bahcall, Schmidt & Gunn 1969) and that at low redshift ($z < 0.4$) they are associated with moderate groups of galaxies (e.g. Fisher et al. 1996). However, little is known at high redshift. Our method yields a mean one-dimensional profile of the density distribution on large scales when other methods study the correlation of the quasar with surrounding objects (see Kauffmann & Haehnelt 2002). This result adds to the growing evidence that high-z QSOs seem to reside in dense and probably highly biased regions (Djorgovski 1999; Djorgovski et al. 1999a). Observational efforts should be done to obtain deep images of the fields around bright high-z quasars to search for the presence of any concentration of objects around the quasar.

ACKNOWLEDGMENTS

REFERENCES

Adelberger K., Steidel C. C., Shapley A., Pettini M., 2003, ApJ, 584, 45
Aguirre A., Schaye J., Theuns T., 2002, ApJ, 576, 1
Aracil B., Petitjean P., Pichon C., Bergeron J., 2004, A&A, 419, 811
Bahcall J. N., Schmidt M., Gunn J. E., 1969, ApJ, 157, L77
Bajtlik S., Duncan R., Ostriker J., 1988, ApJ, 327, 570
Baker A. C., Carswell R. F., Bailey J. A., Espey B. R., Smith M. G., Ward M. J., 1994, MNRAS, 270, 575
Bechtold J. B., 1994, ApJS, 91, 1
Becker G. D., Rauch M., Sargent W. L. W., 2006, preprint (astro-ph/0607633)
Boksenberg A., Sargent W. L. W., Rauch M., 2003, preprint (astro-ph/0307557)
Bruscoli M., Ferrara A., Marri S., Schneider R., Maselli A., Rollinde E., Aracil B., 2003, MNRAS, 343, 41
Carswell R. F., Whelan J., Smith M., Boksenberg A., Tytle D., 1982, MNRAS, 198, 91
Cen R., Mc Donald P., 2002, ApJ, 570, 457
Cen R., Miralda-Escudé J., Ostriker J. P., Rauch M., 1994, ApJ, 437, 6
Cooke A. J., Espey B., Carswell R. F., 1997, MNRAS, 284, 552
Coppolani F. et al., 2006, MNRAS, 370, 1804
Cowie L. L., Songaila A., 1998, Nat, 394, 44
Cristiani S., Vio R., 1990, A&A, 227, 385
Cristiani S., D'Odorico S., Fontana A., Giallongo E., Savaglio S., 1995, MNRAS, 273, 1016
Croft R., 2004, ApJ, 610, 642
Croft R. A. C., Weinberg D. H., Bolte M., Burles S., Hernquist L., Katz N., Kirkman D., Tytler D., 2002, ApJ, 581, 20
Desjacques V., Nusser A., Haehnelt M. G., Stoehr F., 2004, MNRAS, 350, 879
Desjacques V., Nusser A., Sheth R. K., 2007, MNRAS, 374, 206
Djorgovski S. G., 1999, in Bunker A. J., van Breugel W. J. M., eds, ASP Conf. Ser. Vol. 193, The High-Redshift Universe: Galaxy Formation and Evolution at High Redshift. Astron. Soc. Pac., San Francisco, p. 397
Djorgovski S. G., Odewahn S. C., Gal R. R., Brunner R. J., de Carvalho R. R., 1999a, in Weymann R. J., Storrie-Lombardi L. J., Sawicki M., Brunner R. J., eds, ASP Conf. Ser. Vol. 191, Photometric Redshifts and the Detection of High Redshift Galaxies. Astron. Soc. Pac., San Francisco, p. 179
Djorgovski S. G., Gal R. R., Odewahn S. C., de Carvalho R. R., Brunner R., Longo G., Scaramella R., 1999b, in Colombi S., Mellier Y., Raban B., eds, Wide Field Surveys in Cosmology. Editions Frontières, Gif-sur-Yvette, p. 89
Djorgovski S. G., Stern D., Mahabal A. A., Brunner R., 2003, ApJ, 596, 67
Ellison S. L., Songaila A., Schaye J., Pettini M., 2000, AJ, 120, 1175
Faucher-Giguere C.-A., Lidz A., Zaldarriaga M., Hernquist L., 2007, preprint (astro-ph/0701042)
Fernandez-Soto A., Barcons X., Carballo R., Webb J. K., 1995, MNRAS, 277, 235
Ferrarese L., 2002, ApJ, 578, 90
Fisher K. B., Bahcall J. N., Kirhakos S., Schneider D. P., 1996, ApJ, 468, 469
Francis P. J., Hooper E. J., Impey C. D., 1993, AJ, 106, 417
Gaskell C. M., 1982, ApJ, 263, 79
Giallongo E., Cristiani S., D'Odorico S., Fontana A., Savaglio S., 1996, ApJ, 466, 46
Hernquist L., Katz N., Weinberg D. H., 1996, ApJ, 457, 51
Kauffmann G., Haehnelt M., 2002, MNRAS, 332, 529
Kennefick J. D., Djorgovski S. G., de Carvalho R. R., 1995, AJ, 110, 2553
Kim Y.-R., Croft R., 2006, preprint (astro-ph/0701012)
Kollmeier J. A., Weinberg D. H., Davé R., Katz N., 2003, ApJ, 594, 75
Kulkarni V. P., Fall S. M., 1993, ApJ, 413, 63
Liske J., 2003, A&A, 398, 429
Liske J., Williger G. M., 2001, MNRAS, 328, 653
Loeb A., Eisenstein D., 1995, ApJ, 448, 17
Lu L., Wolfe A. M., Turnshek D. A., 1991, ApJ, 367, 19
Lynds R., 1971, ApJ, 164, L73

Magorrian J. et al., 1998, AJ, 115, 2285

Maselli A., Ferrara A., Bruscoli M., Marri S., Schneider R., 2004, MNRAS, 350, 21

McDonald P., Miralda-Escudé J., 2001, ApJ, 549, L11

McDonald P. et al., 2000, ApJ, 543, 1

McDonald P. et al., 2006, ApJS, 163, 80

Murdoch H. S., Hunstead R. W., Pettini M., Blades J. C., 1986, ApJ, 309, 19

Pascarelle S. M., Lanzetta K. M., Chen H.-W., Webb J. K., 2001, ApJ, 560, 101

Petitjean P., Mücket J. P., Kate R. E., 1995, A&A, 295, L9

Pieri M. M., Schaye J., Aguirre A., 2006, ApJ, 638, 45

Prochaska J. X., Gawiser E., Wolfe A., Castro S., Djorgovski S. G., 2003a, ApJ, 595, L9

Prochaska J. X., Castro S., Djorgovski S. G., 2003b, ApJS, 148, 317

Rauch M., 1998, ARA&A, 36, 267

Rees M. J., 1986, MNRAS, 218, 25

Rollinde E., Srianand R., Theuns T., Petitjean P., Chand H., 2005, MNRAS, 361, 1015

Sargent W. L. W., Young P. J., Boksenberg A., Tytler D., 1980, ApJS, 42,41

Scannapieco E., Pichon C., Aracil B., Petitjean P., Thacker R. J., Pogosyan D., Bergeron J., Couchman H. M. P., 2006, MNRAS, 365, 615

Schaye J., Theuns T., Rauch M., Efstathiou G., Sargent W. L. W., 2000, MNRAS, 318, 817

Schaye J., Aguirre A., Kim T.-S., Theuns T., Rauch M., Sargent W. L. W., 2003, ApJ, 596, 768

Schirber M., Miralda-Escudé J., McDonald P., 2004, ApJ, 610, 105

Scott J., Bechtold J., Dobrzycki A., Kulkarni V. P., 2000, ApJS, 130, 67

Scott J., Bechtold J., Morita M., Dobrzycki A., Kulkarni V. P., 2002, ApJ, 571, 665

Sheinis A. I., Bolte M., Epps H. W., Kibrick R. I., Miller J. S., Radovan M. V., Bigelow B. C., Sutin B. M., 2002, PASP, 114, 851

Songaila A., 2004, AJ, 127, 2598

Songaila A., Cowie L., 2002, AJ, 123, 2183

Srianand R., Khare P., 1996, MNRAS, 280, 767

Theuns T., Leonard A., Efstathiou G., Pearce F. R., Thomas P. A., 1998, MNRAS, 301, 478

Tytler D., Fan X. M., 1992, ApJS, 79, 1

Tytler D. et al., 2004, ApJ, 617, 1

Worseck G., Wisotzki L., 2006, A&A, 450, 495

This paper has been typeset from a T$_{\rm E}$X/L$^{\rm A}$T$_{\rm E}$X file prepared by the author.